Characterization of Normal and Infarcted Rat Myocardium Using a Combination of Small-Animal PET and Clinical MRI

Takahiro Higuchi, Stephan G. Nekolla, Antanas Jankaukas, Axel W. Weber, Marc C. Huisman, Sybille Reder, Sibylle I. Ziegler, Markus Schwaiger, and Frank M. Bengel

Nuklearmedizinische Klinik und Poliklinik der Technischen Universität München, Klinikum rechts der Isar, Munich, Germany

The combination of small-animal PET and MRI data provides quantitative in vivo insights into cardiac pathophysiology, integrating information on biology and morphology. We sought to determine the feasibility of PET and MRI for the quantification of ischemic injury in the rat model. **Methods:** Fourteen healthy male Wistar rats were studied with ^{18}F-FDG PET and cine MRI. Myocardial viability was determined in a transmural myocardial infarction model in 12 additional rats, using ^{18}F-FDG PET and delayed-enhancement MRI with gadolinium-diethylenetriaminepentaacetic acid. All PET was acquired with a dedicated small-animal PET system. MRI was performed on a 1.5-T clinical tomograph with a dedicated small-animal electrocardiographic triggering device and a small surface coil. **Results:** In normal rats, ^{18}F-FDG uptake was homogeneous throughout the left ventricle. The lowest mean uptake of the ^{18}F-FDG was found in the apical regions (79% ± 6.0% of maximum) and the highest uptake was in the anterior wall (93% ± 4.3 % of maximum). Myocardial infarct size as determined by histology correlated well with defects of glucose metabolism obtained with ^{18}F-FDG PET (r = 0.89) and also with delayed-enhancement MRI (r = 0.91). Left ventricular ejection fraction in normal rats measured by cine MRI was 57% ± 5.4% and decreased to 38% ± 12.9% ($P <$ 0.001) in the myocardial infarction model. **Conclusion:** Integrating information from small-animal PET and clinical MRI instrumentation allows for the quantitative assessment of cardiac function and infarct size in the rat model. The MRI measurements of scar can be complemented by metabolic imaging, addressing the extent and severity of ischemic injury and providing endpoints for therapeutic interventions.

Key Words: small-animal PET; MRI; rat; myocardial infarction

J Nucl Med 2007; 48:288–294

The need for correlative anatomic imaging has recently been well recognized in PET. Molecular imaging approaches targeting for apoptosis, angiogenesis, hypoxia, receptor density, and gene products have been introduced and applied in animal experimental models (*1*). These techniques are useful to gain an understanding of the early steps of disease development as well as therapeutic effects. The increasing specificity of molecular imaging approaches (hot spot imaging) requires morphologic information for localization and quantification (*2*). PET/CT and SPECT/CT have rapidly gained clinical acceptance, reflecting the diagnostic value of multimodal imaging approaches (*3*). However, CT is associated with considerable radiation exposure, which may be disadvantageous in longitudinal imaging protocols (*4*).

There is great interest in MRI as a noninvasive cardiac imaging modality that can provide precise ventricular morphology with high spatial resolution and good soft-tissue contrast without contrast agents and with no radiation (*5*). The assessment of altered myocardial extracellular space using kinetics of gadolinium-diethylenetriaminepentaacetic acid (Gd-DTPA, Magnevist; Schering AG) (contrast-enhanced MRI [ce-MRI]) has been introduced as a marker of myocardial necrosis in ischemic heart disease (*6,7*). Recently, the feasibility of molecular imaging using nanoparticles has been reported, but the low sensitivity of MRI and the limited availability of contrast agents targeting molecular processes has to be overcome (*8*).

The combination of PET and MRI may add valuable information on cardiac physiology and function and may trace signals addressing molecular and physiologic aspects of disease phenotype and therapeutic effects while minimizing the radiation exposure. Although integrated PET/MRI systems have been suggested recently (*9*), acquiring data on conventional systems and using retrospective image registration appears as a feasible approach in small animals. Dedicated animal MRI systems are costly and are available in only a few imaging laboratories. On the other hand, clinical MRI tomographs are widely available and provide a mature and validated imaging platform to be applied to animal imaging.

The rat is an established experimental animal model for cardiac research. Rat cardiac disease models for human heart failure, myocardial infarction, and myocardial ischemia are frequently used to investigate the disease

Received Jun. 25, 2006; revision accepted Oct. 24, 2006.

For correspondence or reprints contact: Takahiro Higuchi, MD, PhD, Nuklearmedizinische Klinik und Poliklinik der Technischen Universität München, Klinikum rechts der Isar, Ismaninger Strasse 22, 81675 Munich, Germany.

E-mail: higuchi@po2.nsknet.or.jp

pathophysiology or to test the efficacy of new therapies preceding clinical studies (*10–12*). Unlike conventional ex vivo approaches, noninvasive imaging approaches that deal with physiologic and longitudinal observations are expected to provide new perspectives. In particular, the quantification of infarct size with serial examinations may be an attractive surrogate endpoint to test the efficacy of new strategies such as gene and cell therapies. Infarct size is known to be a strong prognostic factor and is expected to be modified by these therapies (*13,14*). However, the small ventricular volume and the high heart rate in normal resting-state rats require high spatial and temporal resolution in small-animal studies.

In this feasibility study, we combined a recently developed small-animal PET system with high sensitivity and resolution (*15,16*) and a clinical 1.5-T MRI system to determine functional and morphologic parameters in the rat heart (glucose metabolism, ce-MRI, and global left ventricular [LV] function). The normal pattern and variability of these parameters were defined, and the feasibility to assess disease alteration was examined using a model of myocardial infarction.

MATERIALS AND METHODS

Experimental Protocol

Experimental protocols were approved by the regional governmental Commission of Animal Protection (Regierung von Oberbayern). Male Wistar rats (Charles River) were used in all experiments. In 14 healthy normal rats (average weight, 316 ± 15 g), ^{18}F-FDG PET and cine MRI studies were performed. To determine the myocardial viability in a transmural myocardial infarction model, ^{18}F-FDG PET, cine MRI, and ce-MRI using gadolinium-DTPA were conducted ($n = 12$).

The left coronary artery (LCA) was ligated to create transmural myocardial infarction. Under anesthesia with intramuscular administration of midazolam (0.1 mg/kg), fentanyl (1 μg/kg), and medetomidin (10 μg/kg) (MMF) and mechanical ventilation, the chest was opened to expose the heart. A 7-0 polypropylene suture on a small curved needle was passed through the LCA and ligated to occlude the LCA. To assess the relationship of in vivo and ex vivo measurements in acute and subacute phases, animals were allowed 1 d ($n = 6$) or 1 wk ($n = 6$) of recovery before MRI. PET was performed within 24 h after MRI. Finally, the heart was excised for ex vivo analysis.

MRI

Rats were anaesthetized with intramuscular administration of MMF during the imaging process. All MRI was performed using a 1.5-T clinical MRI system (Sonata; Siemens Medical Solutions) with a dedicated small-animal electrocardiographic triggering system (SA Instruments) and a small flex loop coil for a human wrist.

For the assessment of LV function, short-axis images were acquired using fast cine imaging with a steady-state free precession (SSFP) sequence (parameters: repetition time, 4.0 ms; echo time, 2.0 ms; flip angle, 80°; interpolated in-plane resolution, 0.42 × 0.41 mm; slice thickness, 2.5 mm with contiguous slices; 13–16 frames per cardiac cycle). After cine MRI, the presence of delayed myocardial enhancement was assessed (ce-MRI) in an infarction model ($n = 12$) at 15 min after intravenous injection of a dose of 0.5 mmol/kg body weight Gd-DTPA. For this purpose, a retrospective segmented inversion recovery–prepared fast low-angle shot pulse (IR-FLASH) was used. The optimal inversion delay for nulling remote myocardium was defined visually in a representative slice. Short-axis views were obtained using the following imaging parameters: repetition time, 850 ms; echo time, 2.6 ms; interpolated in-plane resolution, 0.3 × 0.3 mm; slice thickness, 2.5 mm with contiguous slices; inversion time, 100 ms; and k-space data segmented over 3 cardiac cycles (51 lines/cycle), with data acquired every other cardiac cycle. The sequence was electrocardiographically gated to end diastole.

Quantitative analysis of MRI was performed by a computer program developed at our institution (MunichHeart/MRI) (*17*). Epi- and endocardial contours of the entire LV slices were manually traced in diastole and systole, and the LV volume at end-systolic (ESV) and end-diastolic (EDV) phases as well as LV ejection fraction (LVEF) were calculated. For the definition of the delayed-enhancement area, the percentage of enhanced myocardium in the LV was calculated by manual tracing of enhanced myocardium.

PET Imaging

Anesthesia was initiated and maintained using the same protocol as explained earlier.

Rats received an intravenous injection of ^{18}F-FDG (37 MBq) via the tail vein. Thirty minutes before the ^{18}F-FDG injection, the animals were treated with intraperitoneal administration of insulin (8 mU/g body weight) and glucose (1 mg/g body weight) to enhance tracer uptake into the myocardium. The ^{18}F-FDG imaging acquisition was started 30 min after ^{18}F-FDG administration and continued for 30 min.

PET was performed using a small-animal PET system (MOSAIC; Philips). A full description of the prototype of this system, the A-PET system developed at the University of Pennsylvania, has been published elsewhere (*15,16*). Briefly, the system is based on 14,456 gadolinium oxyorthosilicate (GSO) crystals with dimensions of 2 × 2 × 10 mm. The GSO crystals are glued to a continuous light guide and are read by a hexagonal array of 288 photomultiplier tubes. This gantry design leads to a port diameter of 19.7 cm, a transverse field of view of 12.8-cm diameter, and an axial extent of 12.0 cm. The scanner operates exclusively in 3-dimensional (3D) mode. The coincidence timing window is 12 ns, and the standard energy window lies between 410 and 665 keV. Data were acquired for 12 min, resulting in a sinogram containing the detected coincidences, corrected for randoms.

Sinograms were reconstructed into 128 × 128 matrix (1 × 1 × 1 mm voxel size) transaxial images using the 3D row-action maximum-likelihood algorithm (3D-RAMLA) using a gaussian filter (2-mm full width at half maximum) (*18*). Data corrections included normalization, dead-time, and decay corrections. No corrections were made for attenuation or scatter. Then, volumetric sampling was applied to delineate 3D tracer distributions of ^{18}F-FDG uptake throughout the LV myocardium, and the tracer concentrations of each sampling point were displayed as a polar map (Munich Heart/NM software) (*19*).

Defect size in percentage of LV was defined by the fraction of polar map elements with reduced tracer uptake in the total polar map derived from the ^{18}F-FDG uptake images. The appropriate threshold value for infarct size measurement was determined by using normal values derived from normal rats using ex vivo data as reference.

Ex Vivo Analysis

After the ^{18}F-FDG PET acquisition of infarction model rats, the animals were sacrificed. The hearts were excised, frozen, and embedded in methylcellulose. For histologic analysis, serial short-axis sections in 1-mm intervals (20-μm thickness) of the entire heart were obtained using a cryostat.

For the histologic analysis, hematoxylin–eosin staining was performed on all serial sections (*20,21*). The stained sections were digitized, and the percentage infarct size was analyzed using ImageQuant software (Molecular Dynamics). The LV and the infarct area for each section were manually traced, and the infarction area (as a percentage of the total LV area) was calculated from the summation of each section. Intraobserver and interobserver reproducibilities were $r = 0.99$ (slope = 1.01) and $r = 0.99$ (slope = 1.03) for the infarct size measurement, respectively.

Statistical Analysis

Data are expressed as a mean ± SD. $P < 0.05$ was considered statistically significant. The unpaired *t* test was used to assess the difference in values between normal and infarcted rats. Two comparison analyses were performed with simple linear regression. Multiple group comparisons were performed using ANOVA, which was followed by the Scheffé test to identify differences.

RESULTS

PET and Cine MRI in Normal Rats

Figure 1 displays short-axis images of ^{18}F-FDG uptake in a normal rat heart. LV myocardium showed excellent contrast of ^{18}F-FDG. A polar map of regional distribution and the statistics on 4 segments derived from the 14 normal rats are shown in Figure 2. Almost homogeneous tracer uptake throughout the LV was observed. However, mild differences in uptake were present, with the lowest uptake among the anterior, septal, inferior, and lateral walls being apical ($P < 0.001$).

Short-axis cine MRI from a normal rat at end-diastolic (ED) and end-systolic (ES) phases is shown in Figure 1. The good spatial resolution and soft-tissue contrast provide information about global as well as regional LV and right ventricular wall morphology using the clinical 1.5-T MRI system. Mean EDV, ESV, and LVEF of normal rats were calculated as 0.52 ± 0.09 mL, 0.22 ± 0.06 mL, and 57.2% ± 5.4%, respectively.

Assessment of a Myocardial Infarction Model by ^{18}F-FDG PET, ce-MRI, and Cine MRI

Glucose metabolism assessed by ^{18}F-FDG uptake demonstrated the ischemic injury in the anterior wall of the infarcted rats. ce-MRI showed a regional increased concentration of contrast media in an area corresponding precisely to the ^{18}F-FDG uptake defect (Fig. 3). The infarcted area was confirmed by ex vivo analysis with hematoxylin–eosin staining, revealing a poorly stained region at low magnification.

The comparison between the histologic percentage LV infarct size versus the percentage LV ^{18}F-FDG uptake defect size was performed using different threshold values for ^{18}F-FDG PET. We found linear regression results with correlation coefficients (*r*) ranging from 0.86 to 0.89 with the tested threshold values (3–7 SDs) (Table 1). The smallest difference and the best correlation between infarct size and in vivo findings were observed when 6 SDs below the normal regional mean were used. However, there were few differences between 3 and 6 SDs with regard to the correlation coefficient (0.82 vs. 0.89) (Table 1). An example scatter plot between histologic infarct sizes versus ^{18}F-FDG defect infarct size determined with a threshold of 6 SDs is displayed in Figure 4A. ce-MRI also demonstrated a high correlation of $r = 0.91$ between the histologic percentage LV infarct size versus the percentage LV delayed-enhancement area (Fig. 4B).

Cine MRI showed regional wall motion abnormalities by visual analysis of cine-mode display corresponding to the area with delayed enhancement in all animals. EDV (0.62 ± 0.13 mL) and ESV (0.38 ± 0.12 mL) were significantly higher ($P = 0.036$ and $P < 0.001$, respectively) and LVEF (38.0% ± 12.9%) was significantly lower ($P < 0.001$) in infarction model rats, reflecting the impairment of LV function with myocardial infarction. In addition, LVEF shows a negative correlation with percentage infarct size ($r = 0.73$).

The variability for the measurements of percentage LV infarcted area by both imaging approaches was low, yielding correlation coefficients for intra- and interobserver reproducibility of $r = 0.97$ (slope = 0.98) and $r = 0.97$ (slope = 0.99) for MRI and $r = 0.96$ (slope = 0.87) and $r = 0.97$ (slope = 0.90) for PET, respectively. The intra- and

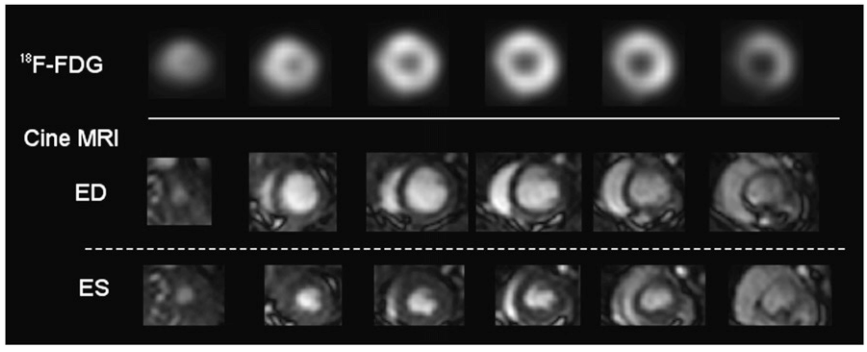

FIGURE 1. Short-axis images of normal rat heart with ^{18}F-FDG uptake and cine MRI at end-diastolic (ED) and end-systolic (ES) phases. Serial images from apex (left) to base (right) are shown.

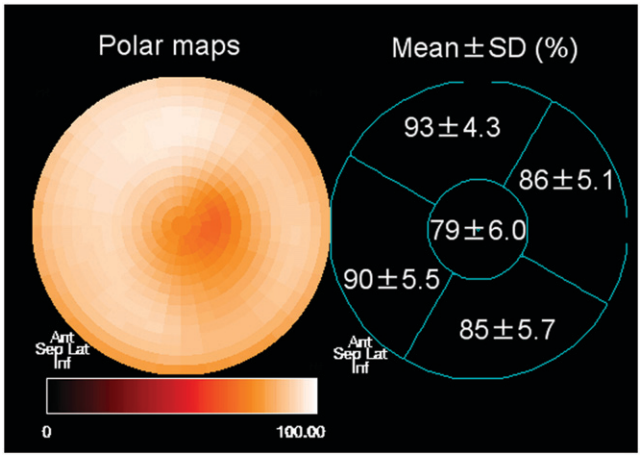

FIGURE 2. Polar maps of normal distributions of ^{18}F-FDG uptake in healthy rats. Mean percentage uptake is almost homogeneous throughout LV wall but slightly decreased at apex. Ant = anterior; Sep = septal; Lat = lateral; Inf = inferior.

interobserver variability of ejection fraction measurements with MRI yielded $r = 0.97$ (slope = 0.87) and $r = 0.98$ (slope = 0.99), respectively.

DISCUSSION

In this study, we combined data from a small-animal PET system and a clinical MRI system for the assessment of glucose metabolism, extent of late enhancement, and global LV function in normal and infarcted rats. Both imaging approaches were highly accurate to determine the extent of myocardial infarction in the rat model.

The feasibility of rat heart imaging with small-animal PET has been previously reported by Kudo et al. (*22*). Our results showing a homogeneous distribution of ^{18}F-FDG in the rat heart and an excellent correlation between ^{18}F-FDG defect and infarct size confirm their findings.

We administrated an insulin/glucose mixture 30 min before ^{18}F-FDG administration to maximize cardiac uptake and to standardize metabolic conditions for all animals. Under normal resting conditions, most energy is derived from long-chain fatty acids in the myocardium. However, the energy source rapidly changes to glucose in response to glucose loading and insulin administration (*23*). In human clinical studies, glucose loading and insulin injection are commonly used to improve image quality and diagnostic accuracy (*24*). All of our study population showed high ^{18}F-FDG uptake in the myocardium, and good image quality was achieved by the applied insulin/glucose stimulation protocol.

High accuracy of the infarct size measurement based on normal distribution patterns was demonstrated without performing attenuation correction. Attenuation correction is one of the important corrections for absolute quantification of PET data in human studies. Fahey et al. reported that attenuation correction is not necessary in rodent studies on the basis of their phantom experiments (*25*). In this study, the observed homogeneous distribution of myocardial activity confirmed this notion. However, slightly decreased ^{18}F-FDG uptake was depicted in the apical segments of

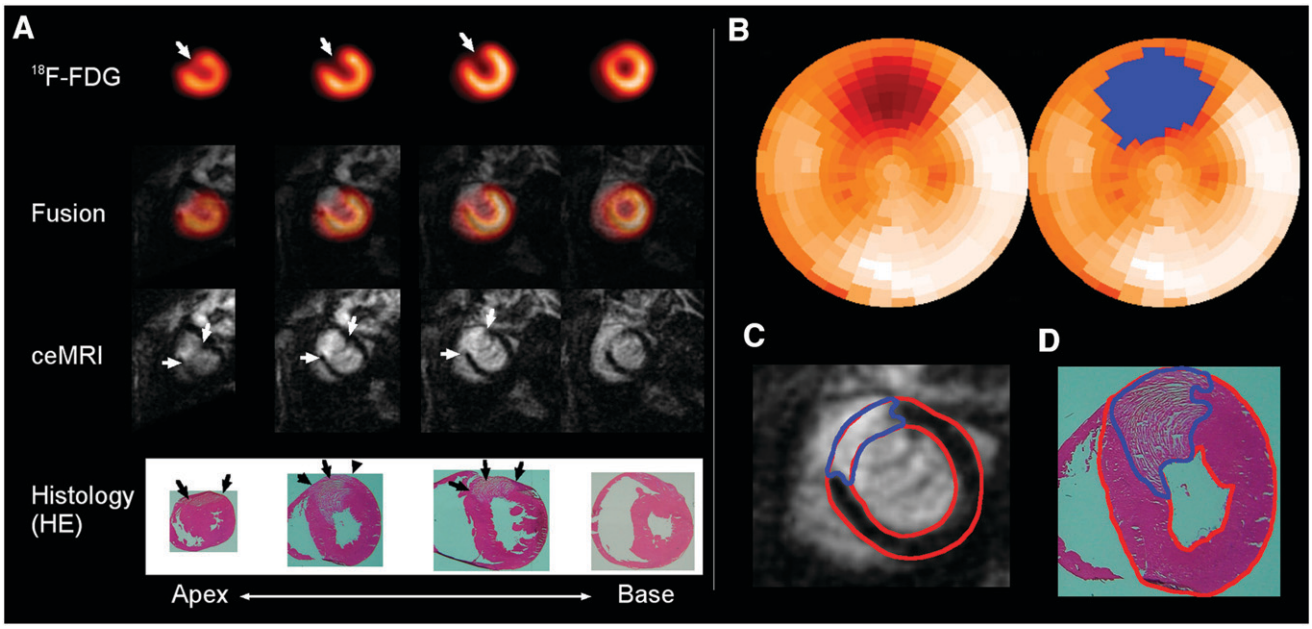

FIGURE 3. (A) Short-axis images from apex (left) to base (right) in rat with permanent left coronary occlusion (1 d after myocardial infarction). ^{18}F-FDG PET shows an uptake defect, and delayed-enhancement MRI (ce-MRI) demonstrates hyperenhanced area in corresponding anterior wall indicated by fused images (arrows). Corresponding histologic sections stained with hematoxylin–eosin reveal the infarct area as a poorly stained area. (B) Polar map views of ^{18}F-FDG uptake (left) and of infarct area (blue) determined by threshold analysis using 6 SDs (right). Examples of tracing of LV region (red) and infarct area (blue) are displayed in C (ce-MRI) and D (histology).

TABLE 1
Correlation Analysis Between Histologic Percentage LV Infarct Size and Percentage LV ^{18}F-FDG Uptake Defect Size Using Different Threshold Values

Threshold value	3 SDs	4 SDs	5 SDs	6 SDs	7 SDs
Mean difference (^{18}F-FDG − histology)	15	8	4	−1	−4
SD of difference	9	8	7	7	6
Slopes (y = ^{18}F-FDG, x = histology)	0.95	1.01	1.03	1.01	0.95
Correlation coefficient	0.82	0.86	0.87	0.89	0.88

normal rats. This is well known in human normal data with PET and SPECT (*26,27*). This heterogeneity is most likely caused by partial-volume effects from apical thinning and motion artifacts occurring in nongated cardiac studies. Acquisition of gated images has to be used to minimize these artifacts in the apical area.

There are few studies performed on an experimental rat infarction model using the MRI enhancement technique to determine infarct size (*20,28,29*). Infarct sizes were reported to vary with time after injection of contrast materials in the case of a fixed inversion delay, and the best time to estimate infarct size has been reported to be approximately 10–16 min. We started measurement of contrast enhancement 15 min after injection and used individually adjusted inversion delays, yielding an excellent correlation (r = 0.91) between the enhancement area and infarct sizes, which is in agreement with other reports (*20,28,29*).

A combination of PET and MRI may represent an ideal platform of noninvasive imaging in small-animal cardiovascular research. In this feasibility study, MRI provided cardiac function and the extent of necrosis, which characterized quantitatively the glucose metabolism in the rat infarction model. Both parameters can serve as surrogate endpoints for therapy status. A permanent occlusion model has been used to validate the imaging signals in comparison with histology in the present study. Figure 5 shows ^{18}F-FDG PET and ce-MRI data in a reperfusion model. ^{18}F-FDG was administrated under a fasting condition 24 h after ischemia/reperfusion. This example indicates the potential of delineating the extent of reversibly injured myocardium by ^{18}F-FDG and the extent of necrosis by ce-MRI. By combining both signals, the extent of ischemic injury can be followed and related to experimental therapies. Additionally, other, more specific molecular tracers may be substituted for ^{18}F-FDG to explore the full potential of integrating MRI-defined morphology with PET-derived biologic signals.

One of the major advantages of MRI for small-animal experiments is its high spatial and temporal resolution that makes it possible to assess the morphology and function of the small ventricle. For targeting of specific molecular events, PET has advantages, with numerous tracers for metabolism, sympathetic function, angiogenesis, hypoxia, and receptors (*1*). Because both techniques have complementary advantages and disadvantages, the combination is very attractive for experimental studies. In addition, it is expected that new methods of data processing will be developed to use

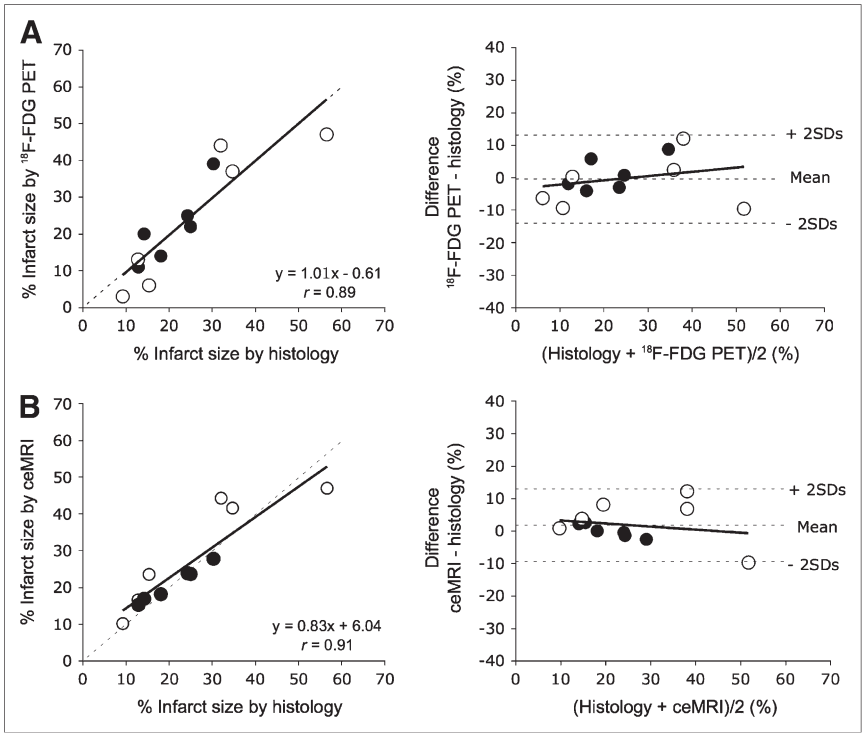

FIGURE 4. Linear regression analysis between percentage LV delayed-enhancement area by ce-MRI and percentage LV infarct size of ex vivo analysis (A) and between percentage LV defect area of ^{18}F-FDG PET (threshold analysis by −6 SDs of normal data base) and percentage LV infarct size (B) in myocardial infarction model of rat. ●, 1 wk after MI; ○, 1 d after MI.

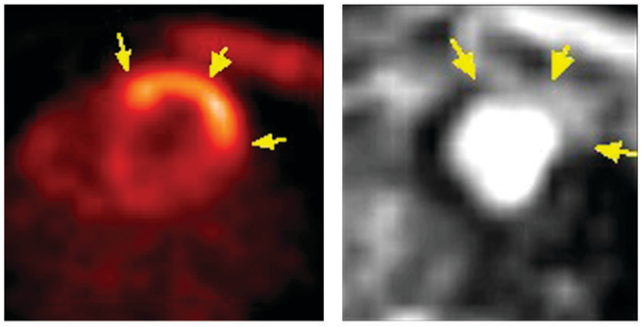

FIGURE 5. Myocardial images of ^{18}F-FDG PET and ce-MRI from a rat with coronary occlusion (20 min), which was followed by reperfusion. ^{18}F-FDG was administrated under a fasting condition 24 h after coronary reperfusion. Increased ^{18}F-FDG uptake is seen (arrow), corresponding to the area of delayed enhancement on ce-MRI (arrow).

MRI data to correct for partial-volume effects in PET and, thereby, improve quantitative measurements (*30*).

In the clinical setting, the combination of PET and CT systems considerably improved the diagnostic performance in oncologic imaging as compared with the separated imaging strategies alone. On the other hand, in terms of cardiovascular examinations, absence of ionizing radiation, good-contrast images of the myocardial wall without contrast agents, the feasibility of cine-mode acquisition, and delayed-enhancement techniques for viability studies are advantages of MRI over CT. This is especially true for small-animal imaging as the required spatial resolution imaging by CT leads to a high radiation exposure in small animals and could potentially affect the results of serial imaging.

Software-based registration of PET and MR images was performed in this study. There is no commercially available instrumentation for simultaneous measurement of PET and MRI. Conventional photomultiplier tubes—used in PET scanners to amplify the photons from the annihilation event—cannot operate in magnetic fields, but alternative technologies such as optical fibers or avalanche photodiode technology are currently being tested in experimental designs (*31,32*).

CONCLUSION

Multiple cardiac tissue and functional parameters in normal and infarcted rats were successfully obtained using the combination of a small-animal PET and a clinical MRI tomograph. The observed correlation with ex vivo measurements confirmed the accuracy of imaging to determine tissue viability and necrosis. A complementary multimodality approach to small-animal imaging may improve the noninvasive characterization of disease phenotype in animal models. The need for quantitative measurements, which can be applied longitudinally for monitoring of therapeutic interventions, is well understood. Multimodality imaging devices are expected to become an integral part of cardiovascular imaging.

ACKNOWLEDGMENTS

The authors are grateful to Dr. Karin Vögele for her data acquisition contribution. The authors thank Dr. Yuri Frenklah and Dr. Ambros Beer for their careful editorial assistance. This study was funded in part by the EC-FP6-project DiMI, LSHB-CT-2005-512146.

REFERENCES

1. Imam SK. Molecular nuclear imaging: the radiopharmaceuticals. *Cancer Biother Radiopharm.* 2005;20:163–172.
2. Quarantelli M, Berkouk K, Prinster A, et al. Integrated software for the analysis of brain PET/SPECT studies with partial-volume-effect correction. *J Nucl Med.* 2004;45:192–201.
3. Schillaci O, Simonetti G. Fusion imaging in nuclear medicine: applications of dual-modality systems in oncology. *Cancer Biother Radiopharm.* 2004;19:1–10.
4. Boone JM, Velazquez O, Cherry SR. Small-animal x-ray dose from micro-CT. *Mol Imaging.* 2004;3:149–158.
5. Constantine G, Shan K, Flamm SD, Sivananthan MU. Role of MRI in clinical cardiology. *Lancet.* 2004;363:2162–2171.
6. Pereira RS, Prato FS, Wisenberg G, Sykes J, Yvorchuk KJ. The use of Gd-DTPA as a marker of myocardial viability in reperfused acute myocardial infarction. *Int J Cardiovasc Imaging.* 2001;17:395–404.
7. Pereira RS, Prato FS, Wisenberg G, Sykes J. The determination of myocardial viability using Gd-DTPA in a canine model of acute myocardial ischemia and reperfusion. *Magn Reson Med.* 1996;36:684–693.
8. Mulder WJ, Strijkers GJ, van Tilborg GA, Griffioen AW, Nicolay K. Lipid-based nanoparticles for contrast-enhanced MRI and molecular imaging. *NMR Biomed.* 2006;19:142–164.
9. Pichler BJ, Judenhofer MS, Catana C, et al. Performance test of an LSO-APD detector in a 7-T MRI scanner for simultaneous PET/MRI. *J Nucl Med.* 2006; 47:639–647.
10. Higuchi T, Taki J, Nakajima K, Kinuya S, Namura M, Tonami N. Time course of discordant BMIPP and thallium uptake after ischemia and reperfusion in a rat model. *J Nucl Med.* 2005;46:172–175.
11. Ott I, Keller U, Knoedler M, et al. Endothelial-like cells expanded from CD34+ blood cells improve left ventricular function after experimental myocardial infarction. *FASEB J.* 2005;19:992–994.
12. Taki J, Higuchi T, Kawashima A, et al. Detection of cardiomyocyte death in a rat model of ischemia and reperfusion using ^{99m}Tc-labeled annexin V. *J Nucl Med.* 2004;45:1536–1541.
13. Gibbons RJ, Valeti US, Araoz PA, Jaffe AS. The quantification of infarct size. *J Am Coll Cardiol.* 2004;44:1533–1542.
14. Schomig A, Kastrati A, Dirschinger J, et al. Coronary stenting plus platelet glycoprotein IIb/IIIa blockade compared with tissue plasminogen activator in acute myocardial infarction: Stent Versus Thrombolysis for Occluded Coronary Arteries in Patients with Acute Myocardial Infarction Study investigators. *N Engl J Med.* 2000;343:385–391.
15. Surti S, Karp JS, Perkins AE, Freifelder R. Design evaluation of A-PET: a high sensitivity animal PET camera. *IEEE Trans Nucl Sci.* 2003;50:1357–1363.
16. Surti S, Karp JS, Perkins AE, et al. Imaging performance of A-PET: a small animal PET camera. *IEEE Trans Med Imaging.* 2005;24:844–852.
17. Ibrahim T, Nekolla SG, Hornke M, et al. Quantitative measurement of infarct size by contrast-enhanced magnetic resonance imaging early after acute myocardial infarction: comparison with single-photon emission tomography using Tc99m-sestamibi. *J Am Coll Cardiol.* 2005;45:544–552.
18. Chiang S, Cardi C, Matej S, et al. Clinical validation of fully 3-D versus 2.5-D RAMLA reconstruction on the Philips-ADAC CPET PET scanner. *Nucl Med Commun.* 2004;25:1103–1107.
19. Nekolla SG, Miethaner C, Nguyen N, Ziegler SI, Schwaiger M. Reproducibility of polar map generation and assessment of defect severity and extent assessment in myocardial perfusion imaging using positron emission tomography. *Eur J Nucl Med.* 1998;25:1313–1321.
20. Flacke S, Allen JS, Chia JM, et al. Characterization of viable and nonviable myocardium at MR imaging: comparison of gadolinium-based extracellular and blood pool contrast materials versus manganese-based contrast materials in a rat myocardial infarction model. *Radiology.* 2003;226:731–738.

21. Degabriele NM, Griesenbach U, Sato K, et al. Critical appraisal of the mouse model of myocardial infarction. *Exp Physiol.* 2004;89:497–505.
22. Kudo T, Fukuchi K, Annala AJ, et al. Noninvasive measurement of myocardial activity concentrations and perfusion defect sizes in rats with a new small-animal positron emission tomograph. *Circulation.* 2002;106:118–123.
23. Cheung JY, Conover C, Regen DM, Whitfield CF, Morgan HE. Effect of insulin on kinetics of sugar transport in heart muscle. *Am J Physiol.* 1978;234:E70–E78.
24. Schoder H, Campisi R, Ohtake T, et al. Blood flow-metabolism imaging with positron emission tomography in patients with diabetes mellitus for the assessment of reversible left ventricular contractile dysfunction. *J Am Coll Cardiol.* 1999;33:1328–1337.
25. Fahey FH, Gage HD, Buchheimer N, et al. Evaluation of the quantitative capability of a high-resolution positron emission tomography scanner for small animal imaging. *J Comput Assist Tomogr.* 2004;28:842–848.
26. Bartlett ML, Bacharach SL, Voipio-Pulkki LM, Dilsizian V. Artifactual inhomogeneities in myocardial PET and SPECT scans in normal subjects. *J Nucl Med.* 1995;36:188–195.
27. Links JM, Becker LC, Anstett F. Clinical significance of apical thinning after attenuation correction. *J Nucl Cardiol.* 2004;11:26–31.
28. Oshinski JN, Yang Z, Jones JR, Mata JF, French BA. Imaging time after Gd-DTPA injection is critical in using delayed enhancement to determine infarct size accurately with magnetic resonance imaging. *Circulation.* 2001;104:2838–2842.
29. Arheden H, Saeed M, Higgins CB, et al. Measurement of the distribution volume of gadopentetate dimeglumine at echo-planar MR imaging to quantify myocardial infarction: comparison with ^{99m}Tc-DTPA autoradiography in rats. *Radiology.* 1999;211:698–708.
30. Bencherif B, Stumpf MJ, Links JM, Frost JJ. Application of MRI-based partial-volume correction to the analysis of PET images of mu-opioid receptors using statistical parametric mapping. *J Nucl Med.* 2004;45:402–408.
31. Marsden PK, Strul D, Keevil SF, Williams SC, Cash D. Simultaneous PET and NMR. *Br J Radiol.* 2002;75(suppl):S53–S59.
32. Pichler BJ, Judenhofer MS, Catana C, et al. Performance test of an LSO-APD detector in a 7-T MRI scanner for simultaneous PET/MRI. *J Nucl Med.* 2006;47:639–647.

JNM The Journal of NUCLEAR MEDICINE

Characterization of Normal and Infarcted Rat Myocardium Using a Combination of Small-Animal PET and Clinical MRI

Takahiro Higuchi, Stephan G. Nekolla, Antanas Jankaukas, Axel W. Weber, Marc C. Huisman, Sybille Reder, Sibylle I. Ziegler, Markus Schwaiger and Frank M. Bengel

J Nucl Med. 2007;48:288-294.

The Journal of Nuclear Medicine is published monthly.
SNMMI | Society of Nuclear Medicine and Molecular Imaging
1850 Samuel Morse Drive, Reston, VA 20190.
(Print ISSN: 0161-5505, Online ISSN: 2159-662X)

SNMMI SOCIETY OF NUCLEAR MEDICINE AND MOLECULAR IMAGING